Barriga, F.J.A.S., Binns, R.A., Miller, D.J., and Herzig, P.M. (Eds.)
Proceedings of the Ocean Drilling Program, Scientific Results Volume 193

9. Data Report: Petrography and Geochemistry of Jasperoids from Site 1189, Ocean Drilling Program Leg 193[1]

R.A. Binns[2,3]

ABSTRACT

Bright red "jasperoids" were recovered at three positions during Leg 193 drilling below Roman Ruins (Site 1189) in the PACMANUS hydrothermal field. These do not represent fossil exhalative oxide deposits equivalent to those associated with sulfide chimneys at the Roman Ruins seafloor. Rather, they constitute an integral, relatively early stage involving oxidized fluids in the development of veins and breccias that characterize the mostly sulfidic stockwork zone intersected below Roman Ruins in Hole 1189B. They formed by growth of quartz in open spaces created by hydrofracturing, the characteristic feature being mostly euhedral cores dusted by tiny hematite flakes. In one occurrence there are also frondlike aggregates and possible earlier cavity linings of hematite, overgrown by quartz, that potentially formed by maturation of ferruginous gels first deposited in the openings. The trace element geochemistry of the jasperoids, apart from minor enrichment in uranium, provides no indication that they represent subsurface conduits for fluids that deposit Fe-Mn-Si at the seafloor, though this remains a possibility for some such deposits.

INTRODUCTION

Sulfide chimneys at the Roman Ruins hydrothermal site in the PACMANUS field, Manus Basin, Papua New Guinea, are accompanied by

[1] Binns, R.A., 2006. Data report: Petrography and geochemistry of jasperoids from Site 1189, Ocean Drilling Program Leg 193. *In* Barriga, F.J.A.S., Binns, R.A., Miller, D.J., and Herzig, P.M. (Eds.), *Proc. ODP, Sci. Results,* 193, 1–30 [Online]. Available from World Wide Web: <http://www-odp.tamu.edu/publications/193_SR/VOLUME/CHAPTERS/211.PDF>. [Cited YYYY-MM-DD]
[2] Division of Exploration and Mining, Commonwealth Scientific and Industrial Research Organisation (CSIRO), PO Box 136, North Ryde NSW 1670, Australia.
Ray.Binns@csiro.au
[3] Department of Earth and Marine Sciences, Australian National University, Canberra ACT 0200, Australia.

Initial receipt: 31 October 2003
Acceptance: 3 November 2004
Web publication: 25 April 2006
Ms 193SR-211

low-lying, intermingled, and fringing deposits of Fe-Mn-Si oxide comprising variable mixtures of Fe oxyhydroxide, opaline silica (commonly with a filamentous microbial structure), and coatings or veinlets of birnessite and todorokite (Binns, Barriga, Miller, et al., 2002; Binns et al., 2002). Similar deposits, overlying dacite and rhyodacite lavas, occur at the Tsukushi and Rogers Ruins sites at PACMANUS, and others occur independently of chimneys at numerous smaller sites in the general vicinity. Some deposits actively vent clear fluids at temperatures in the range 29°–73°C (Binns et al., 2002). Small deposits composed principally of Mn oxide minerals also occur at Tsukushi and the nearby Snowcap site.

During Leg 193 we were alert to the possibility that equivalent fossil Fe-Mn-Si deposits at subsurface paleoseafloor horizons within the volcanic pile might denote earlier phases of hydrothermal activity. No convincing examples were found, but three significant occurrences of bright red hematitic material were encountered during drilling at Roman Ruins (Site 1189; Shipboard Scientific Party, 2002).

These occurrences are closely related to pyrite-bearing breccias and veins abundantly developed at Site 1189. Although superficially resembling jaspers commonly associated with ophiolite complexes and massive sulfide ore deposits, the term "jasperoid" is preferred here to avoid any connotation of an exhalative origin. This report describes investigations of the jasperoids undertaken in order to test their possible relationships to the seafloor oxide deposits at Roman Ruins, in the same sense that the stockwork zone in Hole 1189B represents a likely conduit for sulfide chimney-forming fluids (Shipboard Scientific Party, 2002; **Binns,** this volume).

Details of the samples studied are provided in Table **T1.** The setting of the three jasperoid occurrences within surrounding core material is as follows. The lithologic units cited are those set out in Binns, Barriga, Miller, et al. (2002).

T1. Sample details, p. 28.

Core 193-1189A-7R

A single 3-cm piece of jasperoid with brecciated inclusions of altered country rock, cataloged as lithologic Unit 14 in Hole 1189A, was present at the base of this core. Overlying Unit 13 in Core 193-1189A-7R and underlying Unit 15 in Core 193-1189A-8R both show hydrothermal brecciation and quartz-pyrite veining of pale greenish gray to tan altered volcanic rock, but neither has any development of jasperoid. The relationship between jasperoid and other rock types is therefore unknown for this intersection, although petrographic similarity of the jasperoid to that in the core next described indicates an equivalent nature.

Core 193-1189B-6R

Core 6R from the stockwork zone of Hole 1189B was a partial recovery of rubble, most of which consists of fragments of jigsaw-fit, hydrothermally brecciated, pale greenish gray altered volcanic rock with a fine-grained matrix or stockwork veining of quartz and pyrite (Fig. **F1**). Many fragments contain pods of red jasperoid located centrally in the veins, especially where they broaden into a breccia matrix. Since the rubble was clearly jumbled when extracted from the core liner, separate pieces of massive sulfide and altered amygdaloidal volcanic rock within it were moved to the end of the interval and cataloged as lithologic

F1. Core 19-1189B-6R, p. 10.

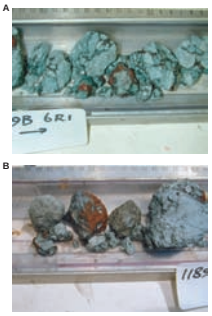

Units 6 and 7, respectively, while the remaining jasperoid-bearing fragments were assigned to Unit 5. Overlying Unit 4 in Core 193-1189B-5R and Unit 8 in underlying Core 193-1189B-7R are both hydrothermally brecciated altered volcanic rocks with stockwork-like matrixes of quartz-pyrite-(anhydrite) vein material. They are broadly similar in appearance to the nonjasperoid parts of Unit 5. This sequence of cores clearly indicates that jasperoid formation is an integral, though only locally developed, component of transgressive quartz veins (normally gray, with sulfides) within the stockwork zone in the upper part of Hole 1189B.

Core 193-1189B-11R

Most of the material recovered in this core comprised long pieces of altered vesicular volcanic rock curated as lithologic Unit 19 and representing commencement of the lower sequence of Hole 1189B (Shipboard Scientific Party, 2002). The upper part of Core 193-1189B-11R unfortunately consisted of fine rubble, containing a single 3-cm piece of red jasperoidal breccia with inclusions of altered wallrock. The remaining fragments in the rubble were of two kinds: breccia with randomly oriented clasts of altered, flow-banded volcanic rock in a quartz matrix with minor magnetite and polymict breccia or volcaniclastic rock with greenish gray, gray, and very pale clasts in a quartz matrix with minor pyrite and magnetite. Neither lithology shows any development of jasperoid. Although somewhat mixed, the two breccia types were, respectively, more abundant on either side of the jasperoid piece when extracted from the core liner. The rubble was rearranged for curating into Units 16 (flow-banded breccia), 17 (jasperoid), and 18 (polymict breccia). There is no certainty this represents the sequence drilled, indeed the rubble could well be derived from collapse higher in the hole. Accordingly, Core 193-1189B-11R provides no definite evidence of the relationship between jasperoid and other rock types. While superficially similar to the other two jasperoid intersections and likely to have the same structural relationship to wallrock, the sample collected from Piece 3 shows important microscopic differences.

METHODS

New thin sections of jasperoid and enclosed wallrock particles were prepared from Samples 193-1189A-7R-1 (Piece 17, 99–102 cm; Commonwealth Scientific and Industrial Research Organization [CSIRO; Australia] 142697), and 193-1189B-11R-1 (Piece 3, 14–16 cm; CSIRO 142714). For the upper jasperoid intersection in Hole 1189B, the shipboard thin section (1189B 16) from nearby Sample 193-1189B-6R-1 (Piece 2, 13–15 cm) was reexamined.

For chemical analysis, representative portions of the three Leg 193 jasperoids, avoiding conspicuous wallrock fragments, were broken or sawn from the samples and the sawn surfaces cleaned with sandpaper. After ultrasonic cleaning and washing in deionized water to remove sea salt, and drying, these subsamples were finely ground under acetone in a mechanical agate mortar and pestle. Analyses were performed by X-ray fluorescence (XRF) spectrometry and by inductively coupled plasma–atomic emission spectrometry (ICP-AES) and mass spectrometry (ICP-MS) using the CSIRO methods outlined in **Miller et al.** (this volume). Loss on drying (LOD; 105°C) and loss on ignition (LOI;

1050°C) were measured gravimetrically on a separate powder aliquot for one sample.

Preferred analyses, taking into account precision and sensitivity of the various methods, are provided in Table T2 together with the average composition of 16 Fe-Mn-Si oxide samples dredged from the seafloor at Roman Ruins. Several outlier analyses were excluded from the latter, as indicated in a table footnote.

T2. Jasperoid compositions, p. 29.

RESULTS

Petrography

The three jasperoid samples from Site 1189 are described in Table T1. Figures F2, F3, F4, F5, F6, F7, F8, F9, F10, F11, F13, F14, F15, and F16 illustrate key petrographic characteristics.

The common feature of the jasperoids is the presence of cores clouded by tiny hematite inclusions within dominant quartz (Figs. F3, F4, F9). The cores are sharply bounded, commonly with outlines indicating a former doubly terminated pseudohexagonal prismatic habit. In Sample 193-1189B-11R-1 (Piece 3, 14–17 cm; CSIRO 142714), there are also strange frondlike aggregates (Fig. F12) and possible earlier cavity linings (Fig. F14) of hematite, overgrown by quartz. The hematite flakes are too small to display diagnostic optical properties, but are identified as such by their bright red internal reflections that are particularly strong when observed in reflected light with crossed polarizers. However, some more yellowish brown flakes in the frond structures may be goethite.

Quartz grains vary in overall size between the samples and range from seriate where closely packed to euhedral where separated by open pores or microdrusy cavities. Larger druses, and in one case an open fracture, are lined by well-crystallized quartz generally free of hematite inclusions (implying crystallization from a more reduced fluid). Euhedral pyrite, subordinate overgrowths of anhydrite, and very rare globules of clay also line or fill some cavities. Some disseminated pyrite euhedra and subhedra, most distinctly larger than the jasperoidal quartz, are not so clearly related to drusy structures and may have formed by replacement of quartz matrix after passage of H_2S-bearing fluid. There are no distinct boundaries between quartz with hematitic cores in the main body of the jasperoids and quartz lining the cavities, the latter apparently representing a continuation of the same quartz crystallization episode as the margins of jasperoidal grains.

Thin selvages of clear quartz surround wallrock fragments in two of the samples (Figs. F2, F6, F8), although in Core 193-1189B-6R (Fig. F1) they are present in analyzed Piece 5 (Fig. F8) but lacking in sectioned Piece 2 nearby (Fig. F10). These selvages also appear to be continuous outgrowths from the jasperoidal quartz (Fig. F7), but at the immediate contacts they may show grain-scale jagged replacement of wallrock.

Narrow veinlets of selvage quartz (Fig. F7) or, where selvages are lacking, of jasperoidal quartz with varying hematite abundance (Figs. F10, F11) locally cut into or across the wallrock fragments. Adjacent to these there may be some silicification of wallrock by poikiloblasts of quartz (with numerous clay inclusions) that tend to have epitaxial orientations relative to adjacent vein quartz (Fig. F10). One such veinlet fills a dilated microfracture that wedged apart a plagioclase phenocryst in wallrock (Fig. F10).

F2. Jasperoid piece, p. 11.

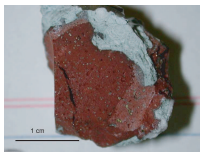

F3. Jasperoid grain size, p. 12.

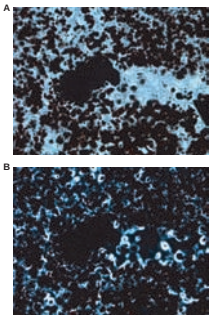

F4. Enlarged view of grain size, p. 13.

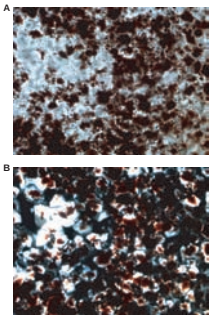

F5. Late-stage fractures, p. 14.

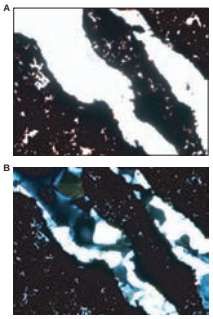

The shapes of wallrock fragments are very irregular (Figs. F2, F8), too much so to permit their reconstruction as a simple jigsaw-fit hydrothermal breccia. Sample 193-1189B-6R-1 (Piece 2, 13–15 cm) contains a variety of fragments with differing microfabrics, some perlitic, some with more massive fabrics, and some vesicular. Evidently they have been mixed together by brecciation or hydrofracturing from separate, though conceivably adjacent, sources and their outlines modified by solution or replacement. Similar features occur in many sulfide-rich, nonjasperoidal quartz veins or breccia matrixes in adjacent core pieces.

Geochemistry

The three jasperoid samples are composed primarily of Si, Fe, and S (Table T2), together with minor Ca attributable to anhydrite and traces of other lithophile (normally "major") elements (Ti, Al, Mg, Na, and K, but not P) likely to be mainly present in small wallrock fragments unavoidably left in the analyzed powders. Manganese contents are particularly low. Table T3 lists normative mineralogy computed by allocating S (after calculating anhydrite abundance from Ca) with Cu and Fe to chalcopyrite then with Fe to pyrite. The abundance of hematite, calculated from residual Fe, is comparatively small in all samples, while quartz is by far the dominant normative component. Normative proportions of pyrite and lesser chalcopyrite in two samples agree with microscope observations. As evident modally, normative anhydrite is most abundant yet still minor in Sample 193-1189B-11R-1 (Piece 3, 14–16 cm; CSIRO 142714). Wallrock contaminants (computed from Al_2O_3, with reference to nearby wallrock samples) amount to 2–3 wt%.

Detailed discussion of wallrock compositions is not justified given their small contribution, possible analytical errors, and the assumptions made in normative calculations, but their Ti/Al ratio is lower by a factor of ~2 relative to altered volcanic rocks analyzed by the author from nearby cores. This, together with their apparent Cr content, suggests somewhat more mafic dacite parents.

Phosphorous contents are higher than likely wallrock contributions in jasperoid Samples 193-1189A-7R-1 (Piece 17, 99–102 cm; CSIRO 142697) and 193-1189B-11R-1 (Piece 3, 14–16 cm; CSIRO 142714) by a factor of ~50, these being the two samples where trace apatite was noted (Figs. F6, F13). LOI for the single Sample 193-1189A-7R-1 (Piece 17, 99–102 cm; CSIRO 142697), where this was determined, is inexplicably high, more so than expected to arise from wallrock contaminants, misidentification of goethite, rare observable fluid inclusions, or absence of an adjustment for pyrite oxidation, which would cause gain on ignition. Low analytical totals for the other two samples (Table T1) hint at a similar problem.

Applying data obtained from nearby altered wallrock samples to the normative ratios, the lithophile trace elements V, Ga, and Th are explicable by the presence of wallrock contaminants. Li, however, is distinctly enriched (~×500), while Rb (~×5), Cs (~×5 to ×10), and, in two samples, the rare earth elements (REE) (see below) are moderately enriched. The mineralogical habitat of apparent excess Li, Rb, and Cs in the jasperoid is undetermined. U is distinctly enriched (~×30) in Sample 193-1189A-7R-1 (Piece 17, 99–102 cm; CSIRO 142697) and ~×200 in Sample 193-1189B-11R-1 (Piece 3, 14–16 cm; CSIRO 142714), and slightly so (~×5) in Sample 193-1189B-6R-1 (Piece 5, 45–55 cm; CSIRO 142707), correlating with P (apatite?) abundance. Though their levels in the jasperoids are low, Sr (~×20) and Ba (~×4) are significantly en-

F6. Jasperoid wallrock fragment contact, p. 15.

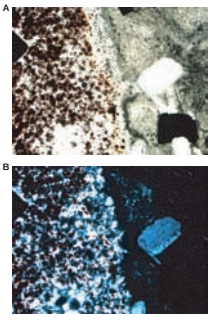

F7. Enlarged view of contact, p. 16.

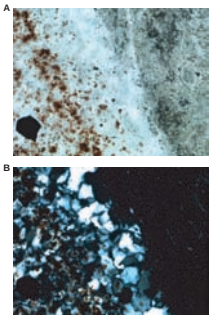

F8. Sawn surface, p. 17.

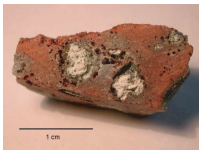

F9. Coarse-grained jasperoid, p. 18.

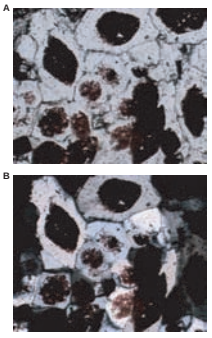

F10. Jasperoid-altered wallrock fragment contact, p. 19.

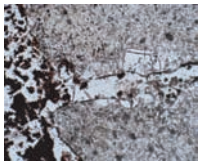

riched only in Sample 193-1189B-11R-1 (Piece 3, 14–16 cm; CSIRO 142714) with the higher anhydrite content, but are explicable as wallrock contaminant in the other samples.

Chondrite-normalized REE profiles for the jasperoids (Fig. F17A) show two contrasting patterns. Relative to the other jasperoids, Sample 193-1189B-6R-1 (Piece 5, 45–55 cm; CSIRO 142707) has lower REE abundances and no pronounced Eu anomaly. Altered wallrocks at Site 1189 mostly show distinctly negative Eu anomalies (Fig. F17B), and it is difficult to account for the jasperoid REE patterns by wallrock contaminants in the samples. Bach et al. (2003) report highly variable REE abundances and chondrite-normalized patterns for vein anhydrites, with both positive and negative Eu anomalies. Considering their minor anhydrite content, REE abundances in this mineral do not explain the jasperoid patterns. It appears that the REE in Samples 193-1189A-7R-1 (Piece 17, 99–102 cm; CSIRO 142697) and 193-1189B-11R-1 (Piece 3, 14–16 cm; CSIRO 142714) particularly are contained mainly in another component, possibly apatite.

Apart from Cu, chalcophile trace elements have low and variable abundances in the jasperoids, but Co, Ni, Zn, Ge, As, Mo, In, Sb, Te, Tl, Pb, and Bi contents are, in most cases, all higher than expected from wallrock contributions by factors ranging from ×10 to ×500. Except for In, which is higher in the chalcopyrite-bearing samples, there is no clear correlation with observed sulfide abundances. Elevated Cd in Sample 193-1189B-11R-1 (Piece 3, 14–16 cm; CSIRO 142714) is accompanied by elevated Zn, possibly arising from sphalerite overlooked under optical microscope.

DISCUSSION

Origin of the Jasperoids

The setting of jasperoids at Site 1189, as matrixes to breccias cutting altered volcanic wallrock (Fig. F1), precludes any likelihood they represent fossil exhalative Fe-Si deposits comparable with those associated with chimneys at the Roman Ruins seafloor. Their overall microfabric, particularly their possession of numerous drusy cavities and microcavities, is similar to that displayed by many quartz-rich veins and breccia matrixes nearby in the generally sulfidic stockwork zone intersected from the base of casing at 30 to ~100 meters below seafloor (mbsf) in Hole 1189B (Shipboard Scientific Party, 2002). The prominent difference between jasperoids and associated nonjasperoidal veins is the presence of early formed hematite-rich cores in jasperoid quartz grains and crystals, indicating an earlier phase of quartz growth from relatively oxidized hydrothermal fluids. In Sample 193-1189B-11R-1 (Piece 3, 14–16 cm; CSIRO 142714), frondlike and botryoidal aggregates of hematite (and possibly goethite) do not resemble the microbial filamentous structures common in seafloor Fe-Mn-Si deposits at Roman Ruins and reported from certain oxide deposits at modern submarine hydrothermal vents and in ancient ferruginous cherts and jaspers associated with massive sulfide ore deposits (Juniper and Fouquet, 1988; Duhig et al., 1992; Grenne and Slack, 2003). Conceivably, they formed by maturation of ferruginous gels, overgrown by quartz.

The tendency for jasperoid to occur centrally in veins and jogs within breccia (Fig. F1) would conventionally be interpreted to suggest late formation. However, petrographic features, including the clear

F11. Jasperoid vein, p. 20.

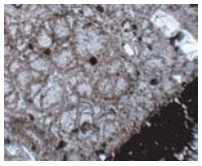

F12. Hematite growths, p. 21.

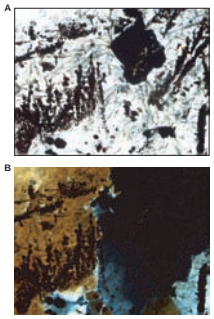

F13. Enlarged view of hematite, p. 22.

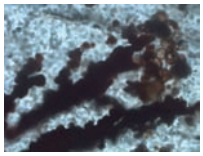

F14. Hematite and oval growth, p. 23.

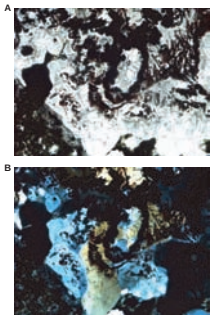

F15. Euhedral growth structure, p. 24.

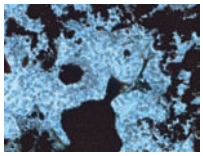

quartz selvages on wallrock fragments locally extending as dilational veins into the latter, are more consistent with early crystallization of the jasperoidal quartz, perhaps at the initial stages of hydrothermal brecciation. The later selvages and veins possibly continue along Core 193-1189B-11R and adjacent cores to form more typical nonjasperoidal breccias, generally richer in pyrite, of the stockwork zone in Hole 1189B. Unfortunately, the thin section studied of Sample 193-1189B-11R-1 (Piece 3, 14–16 cm; CSIRO 142714) does not cover the full transition, and the jumbled nature of the rather poor core recovery renders this difficult to establish conclusively.

None of the jasperoidal or sulfidic quartz veins show crack-seal structures indicative of tectonic origin. Rather, they appear to have crystallized relatively rapidly and largely unimpeded within open spaces created by dilational hydrofracturing, leaving numerous small drusy cavities, but with limited replacement and silicification of enclosed wallrock fragments. The process was episodic, with an earlier generation of quartz crystallizing from oxidized Fe-bearing solutions simultaneously depositing hematite flakes on the expanding quartz surfaces and overgrowing some previously formed hematite aggregates.

This was followed fairly abruptly by continued growth, under more reduced conditions inhibiting hematite precipitation, of the clear margins on jasperoidal quartz grains, the linings to drusy cavities, and the selvages around wallrock fragments plus veinlets within them causing localized silicification. Pyrite crystallized within remnant cavities late in the sequence or replaced the jasperoid quartz, while limited anhydrite finally crystallized as overgrowths in or fillings of cavities. The pyrite is unlikely to be in equilibrium with hematite, having formed distinctly later as fluids became more reduced and sulfurous.

Relationships to Seafloor Fe-Mn-Si Deposits at Roman Ruins

The jasperoids lack Mn and have Si/Fe ratios distinctly higher than those of ferruginous exhalative deposits at the Roman Ruins seabed, apart from a few composed mainly of biogenic opaline silica (Fig. **F18;** Table **T2**). Relative to Fe contents they share enriched U, but the jasperoids are lacking in Zn, As, Sb, and Pb. Their REE abundances fall within the variable range displayed by seabed Fe-Mn-Si deposits at Roman Ruins (Fig. **F17C**), wherein REE abundances broadly correlate with Fe content, but their Eu anomalies are subdued by comparison and for two jasperoid samples the chondrite-normalized patterns differ by virtue of light REE depletion. Comparative geochemistry thus provides no definitive support for any contention that the jasperoids reflect subsurface passage of oxidized fluids depositing Fe-Mn-Si oxides at the seafloor, although the shared enrichment in U deserves note in that respect. Presence of Mn (a dominant component with Fe in chimney vent fluids) and elevated Zn, As, and Sb contents (elements also abundant in sulfide chimneys) instead suggest that the Fe-Mn-Si deposits at Roman Ruins precipitate from expiring chimney-forming fluids that cooled and deposited their sulfide load close to the seafloor. Nevertheless, the jasperoids establish that oxidized fluids passed through the stockwork zone of Hole 1189B and breccia zones in Hole 1189A at an early stage in their development, so it remains possible that some ferruginous oxide deposits on the seafloor formed as a consequence.

F16. Wallrock fragment, p. 25.

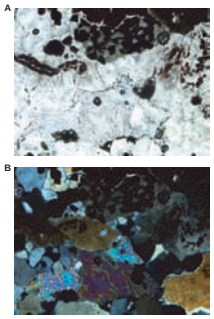

T3. Normative compositions, p. 30.

F17. REE patterns, p. 26.

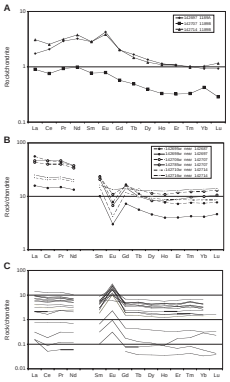

F18. Jasperoid vein composition, p. 27.

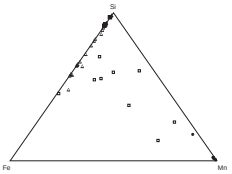

ACKNOWLEDGMENTS

Lesley Dotter and Mike Hart of CSIRO performed the ICP and XRF analyses, respectively. This research used samples provided by the Ocean Drilling Program (ODP). ODP is sponsored by the U.S. National Science Foundation (NSF) and participating countries under management of Joint Oceanographic Institutions (JOI), Inc. Funding was provided by CSIRO and the P2+ consortium of Australian mineral companies.

REFERENCES

Bach, W., Roberts, S., Vanko, D.A., Binns, R.A., Yeats, C.J., Craddock, P.R., and Humphris, S.E., 2003. Controls of fluid chemistry and complexation on rare earth element contents of anhydrite from the PACMANUS subseafloor hydrothermal system, Manus Basin, Papua New Guinea. *Miner. Deposita,* 38(8):916–935.

Binns, R.A., Barriga, F.J.A.S., Miller, D.J., et al., 2002. *Proc. ODP, Init. Repts.,* 193 [CD-ROM]. Available from: Ocean Drilling Program, Texas A&M University, College Station TX 77845-9547, USA. [**HTML**]

Binns, R.A., McConachy, T.F., Parr, J.M., and Yeats, C.J., 2002. The PACMANUS Memoir (P2+). *CSIRO Exploration and Mining Report* 1032C [CD-ROM]. Available from: CSIRO Exploration and Mining, North Ryde NSW 1670, Australia.

Duhig, N.C., Stolz, J., Davidson, G.J., and Large, R.R., 1992. Cambrian microbial and silica gel textures in silica iron exhalites from the Mount Windsor volcanic belt, Australia: their petrography, chemistry and origin. *Econ. Geol.,* 87:764–784.

Grenne, T., and Slack, J.F., 2003. Bedded jaspers of the Ordovician Løkken ophiolite, Norway: seafloor deposition and diagenetic maturation of hydrothermal plume-derived silica-iron gels. *Miner. Deposita,* 38:625–639.

Juniper, S.K., and Fouquet, Y., 1988. Filamentous iron-silica deposits from modern and ancient hydrothermal sites. *Can. Mineral.,* 26:859–869.

Shipboard Scientific Party, 2002. Site 1189. *In* Binns, R.A., Barriga, F.J.A.S., Miller, D.J., et al., *Proc. ODP, Init. Repts.,* 193 [CD-ROM]. Available from: Ocean Drilling Program, Texas A&M University, College Station TX 77845-9547, USA. [**HTML**]

Figure F1. (**A**) Upper and (**B**) lower portions of Core 193-1189B-6R (79.0–88.7 mbsf) photographed immediately after extraction from the core liner. Top is to the right. Red jasperoid occurs as central patches in a network of quartz-(pyrite) veins cutting brecciated and altered dacite wallrock. When curating this rubble, a lump (Piece 6, Unit 6) of massive pyrite (just right of center in B) was moved to the left of (i.e., below) the adjacent jasperoid fragment (Piece 5, used for chemical analysis). Amygdaloidal Piece 7 at the far left of B was assigned to Unit 7, and the remainder of the core to Unit 5. Shipboard thin section 1189 116 was prepared from the fragment (curated as Piece 2) at 12–14 cm below the inverted scale in A.

A

B

Figure F2. Portion of the single jasperoid piece recovered in Hole 1189A (Sample 193-1189A-7R-1 [Piece 17, 99–102 cm; CSIRO 142697]). The jasperoid, containing scattered pyrite grains and small irregular cavities lined by quartz crystals, forms the matrix in a breccia with disoriented fragments of altered perlitic wallrock. Narrow selvages of colorless quartz surrounding the wallrock fragments appear continuous with thin quartz veins (not visible) cutting both jasperoid and wallrock. The prominent fracture on the left is lined with inclusion-free drusy quartz and rare blades of anhydrite. Paler red areas are unpolished saw cuts.

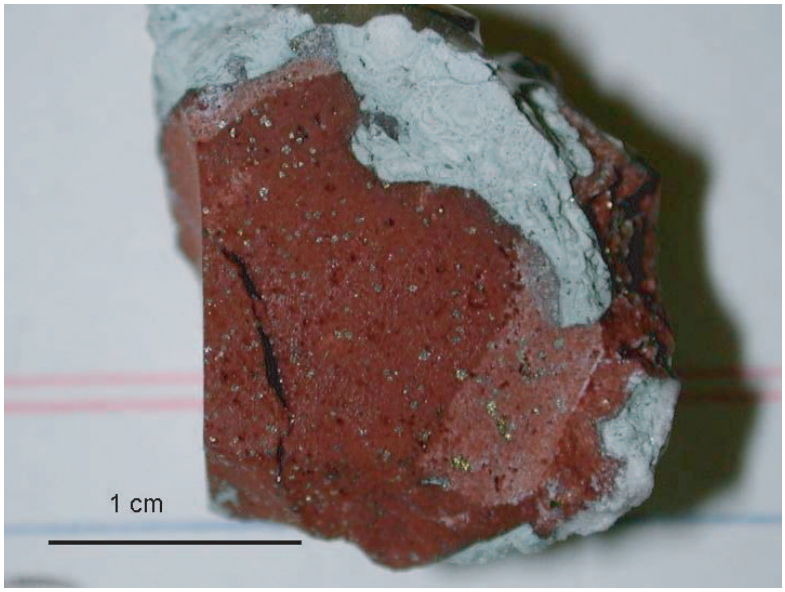

Figure F3. Typical fine grain size and fabric of jasperoid in Sample 193-1189A-7R-1 (Piece 17, 99–102 cm; CSIRO 142697; see Fig. F2, p. 11) consisting of quartz grains with cores clouded by numerous hematite inclusions. Quartz grains adjacent to numerous drusy microcavities possess smaller cores and euhedral habits. A large anhedral pyrite occurs just left of center. Width of view = 1.3 mm. **A.** Ordinary light. **B.** Crossed polarizers.

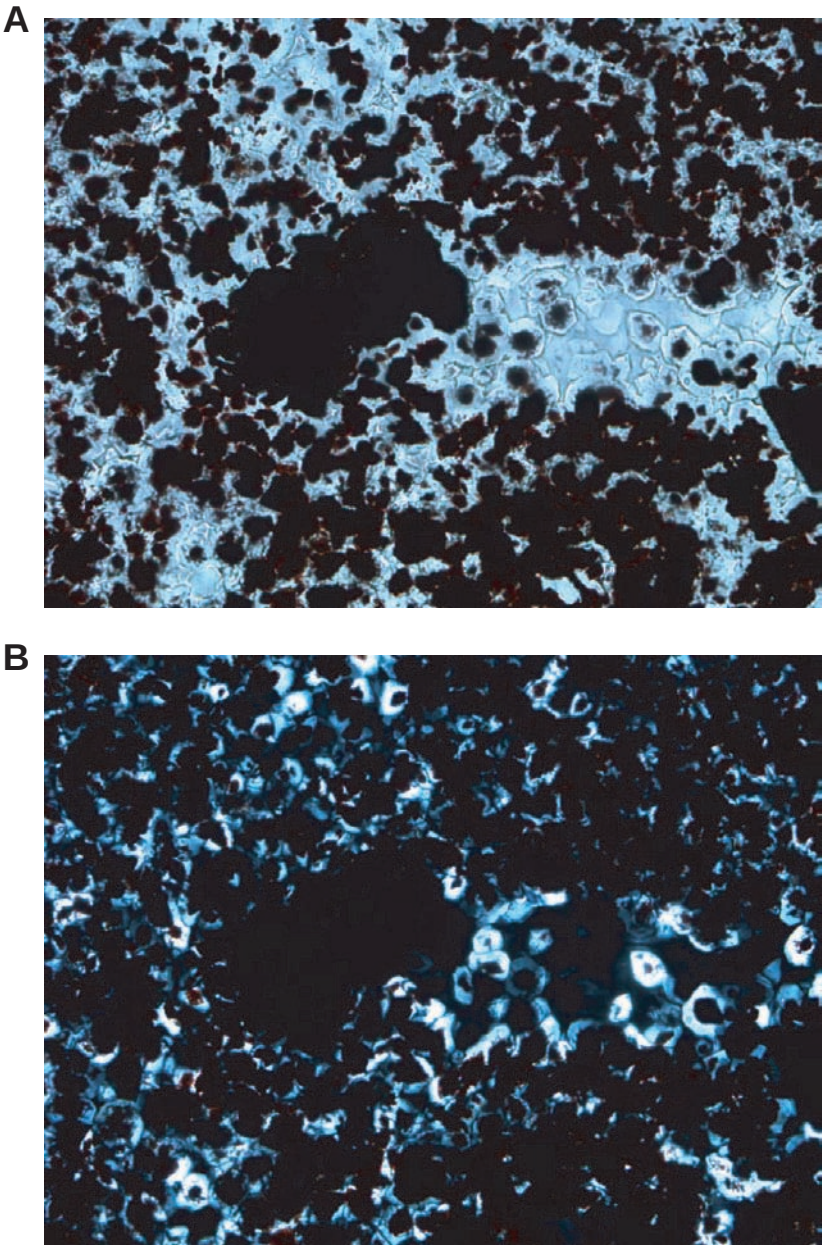

Figure F4. Enlarged view of Sample 193-1189A-7R-1 (Piece 17, 99–102 cm; CSIRO 142697; see Fig. F3, p. 12) in thin section showing platy nature of hematite inclusions in quartz. A small drusy cavity occurs at the left. Width of view = 0.64 mm. **A.** Ordinary light. **B.** Crossed polarizers.

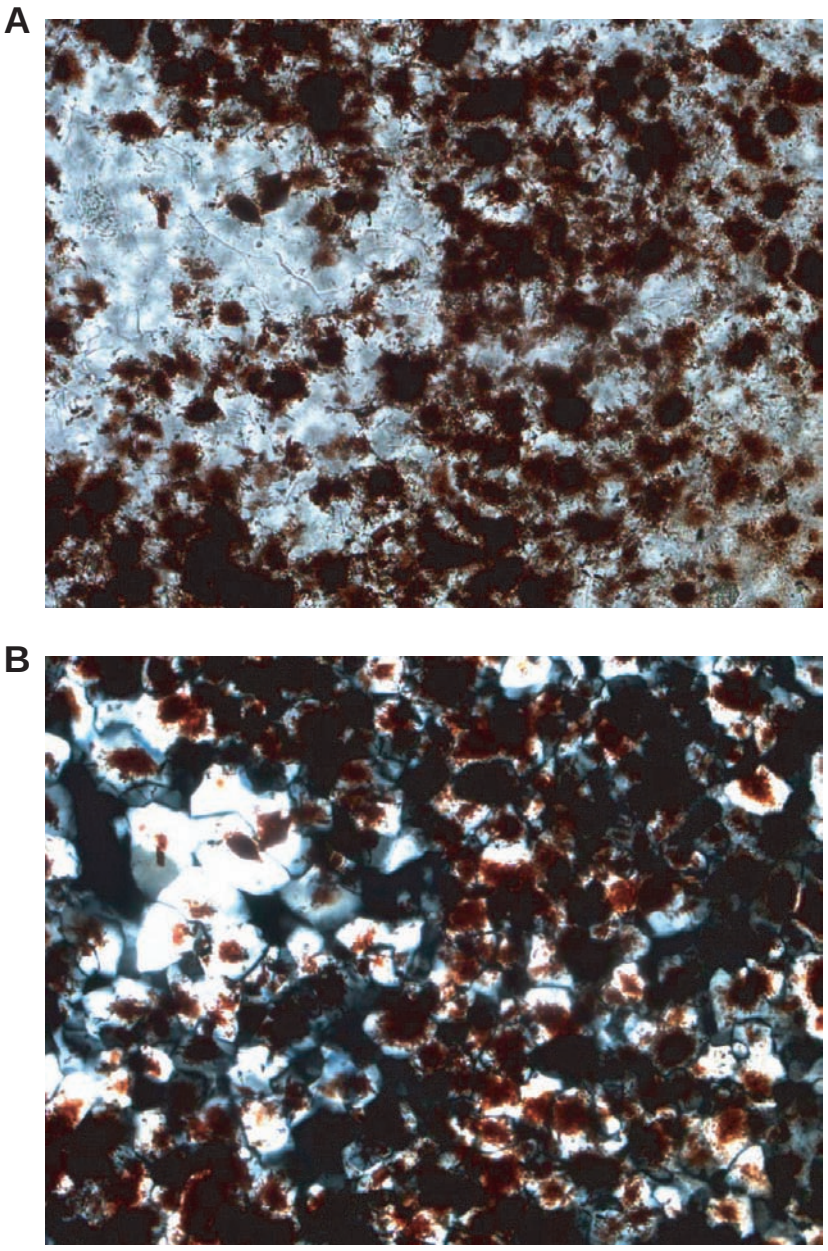

Figure F5. Late stage fractures through jasperoid portion of Sample 193-1189A-7R-1 (Piece 17, 99–102 cm; CSIRO 142697; see Fig. F2, p. 11) lined by coarse-grained quartz with local euhedral terminations. **A.** Ordinary light. **B.** Crossed polarizers. Most blue-gray areas in B are epoxy fill in the drusy-like fracture. Width of field = 1.3 mm.

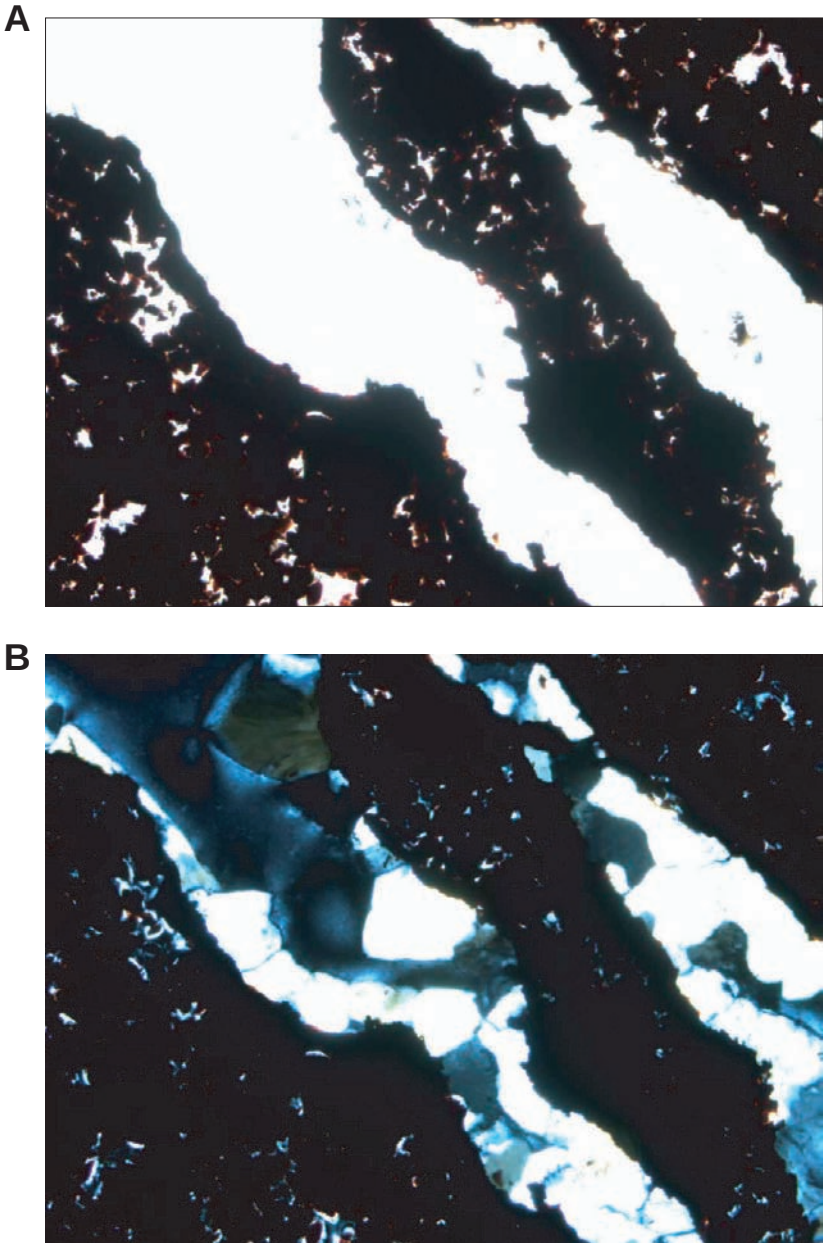

Figure F6. Contact between jasperoid and a wallrock fragment in Sample 193-1189A-7R-1 (Piece 17, 99–102 cm; CSIRO 142697) marked by a selvage of quartz lacking hematite cores. Large pyrite cubes occur in both jasperoid and wallrock. The wallrock contains corroded phenocrysts of unaltered plagioclase and numerous plagioclase microlites set in clay. Tiny crystals of probable apatite occur in the upper part of the selvage; these are rare overall in the sample. Width of field = 1.3 mm. **A.** Ordinary light. **B.** Crossed polarizers.

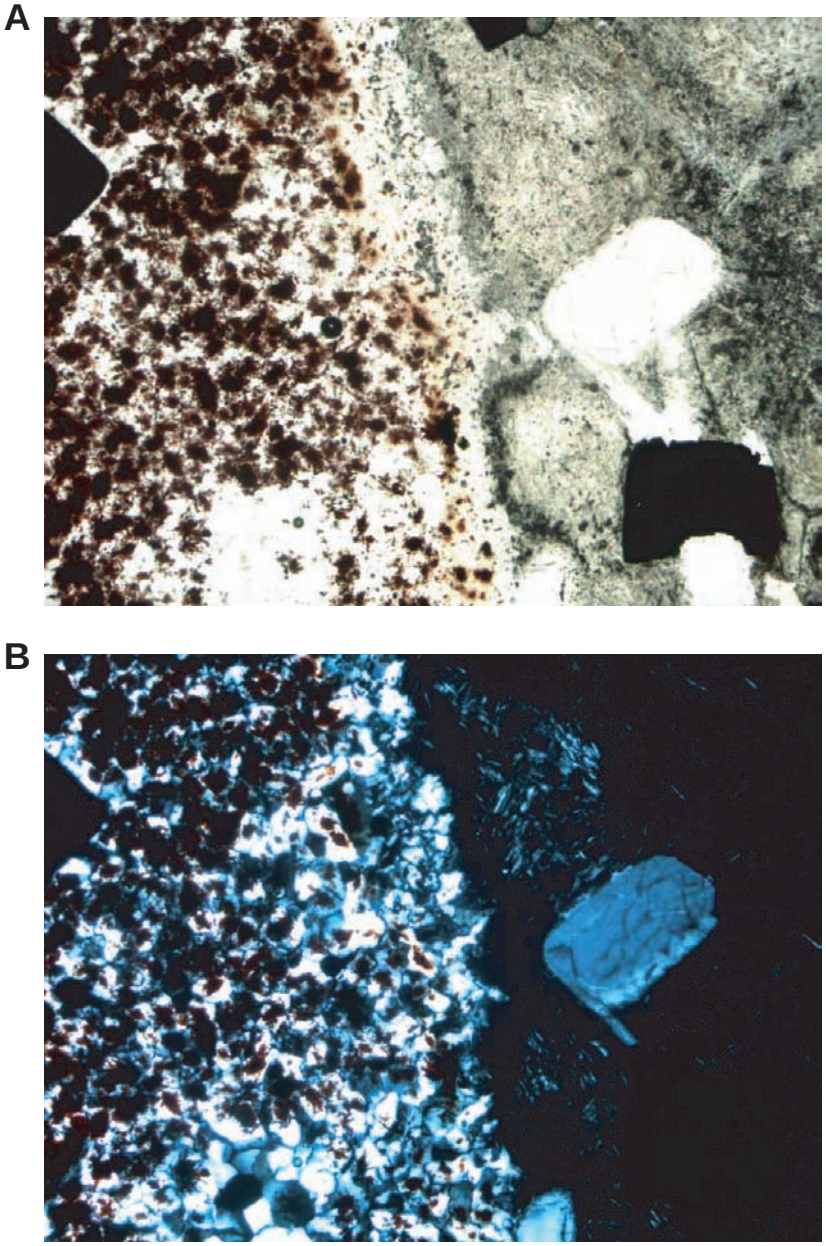

Figure F7. Enlarged view of a contact between jasperoid and wallrock in Sample 193-1189A-7R-1 (Piece 17, 99–102 cm; CSIRO 142697). The selvage of inclusion-free quartz appears to have grown continuously with the clear outgrowths of quartz grains within the jasperoid portion (left), whereas its jagged boundary against wallrock suggests replacement of the latter. A thin quartz veinlet in wallrock extends vertically from the selvage at an irregularity in the boundary. Within the jasperoid, there is a banding in the proportion of hematite; this is uncommon. Width of view = 0.64 mm. **A.** Ordinary light. **B.** Crossed polarizers.

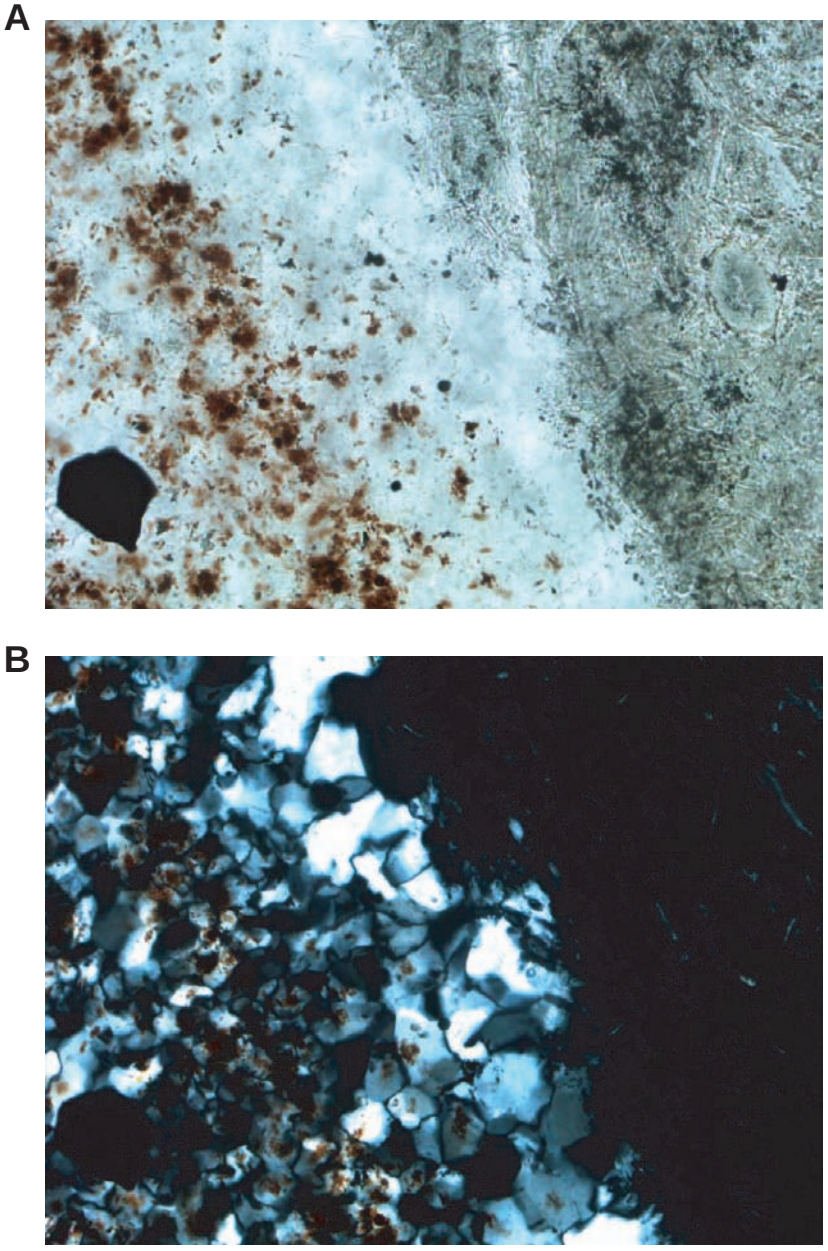

Figure F8. Sawn surface of jasperoid Sample 193-1189B-6R-1 (Piece 5, 45–55 cm; CSIRO 142707; see Fig. F1B, p. 10), showing altered perlitic wallrock fragments and conspicuous cavities. Pale smoky quartz forms selvages around the wallrock fragments and also occurs as patches surrounding drusy cavities (far left). The smoky quartz selvage to the lower wallrock fragment also extends internally as an apparently replacive vein. Disseminated pyrite is scarce.

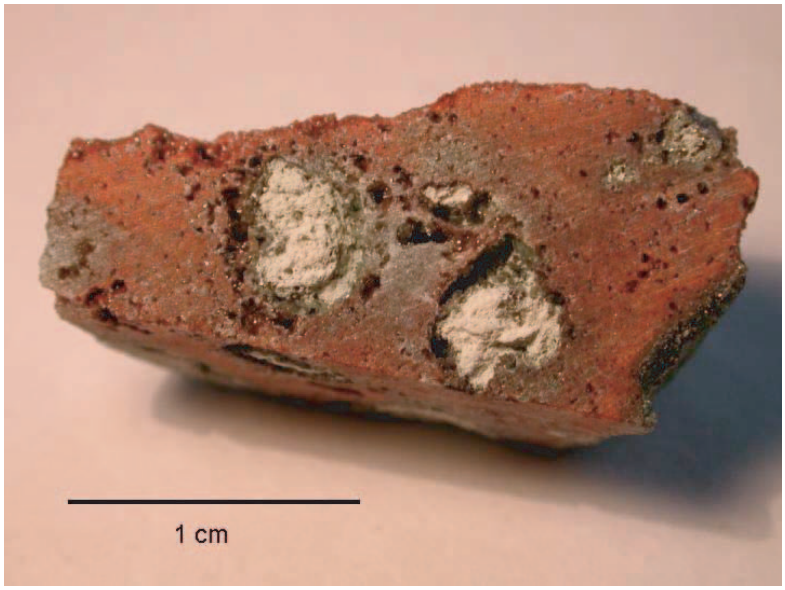

Figure F9. Typical fabric of relatively coarse grained jasperoid in Sample 193-1189B-6R-1 (Piece 2, 13–15 cm), comparable with CSIRO Sample 142697 at 45–55 cm (see Fig. F8, p. 17), showing interlocking quartz grains with sharply defined cores containing numerous inclusions of tiny hematite flakes. Some cores display shapes resembling subhedral, doubly terminated quartz prisms. Strain extinction in some clear quartz overgrowths suggests growth interference. Width of view = 1.4 mm. **A.** Ordinary light. **B.** Crossed polarizers.

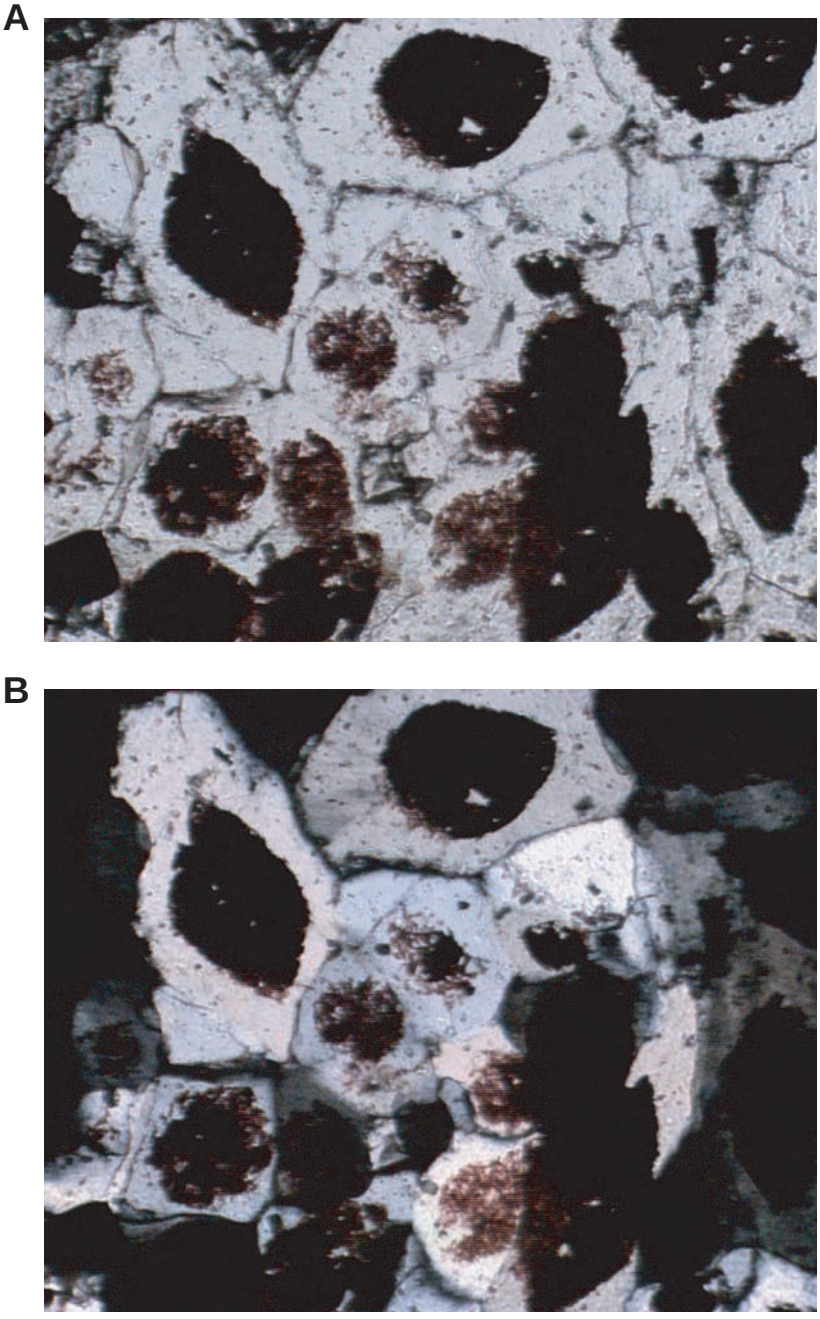

Figure F10. Contact between jasperoid and altered wallrock fragment in Sample 193-1189B-6R-1 (Piece 2, 13–15 cm) showing a veinlike extension of the jasperoid cutting the wallrock and separating a phenocryst of unaltered plagioclase. Immediately adjacent to the vein, the clay-rich wallrock has been silicified by poikiloblastic quartz patches with epitaxial orientations relative to vein quartz grains. Some wallrock fragments have been replaced by scattered prismatic quartz crystals with similar poikiloblastic outgrowths. There is no selvage of inclusion-free quartz at wallrock contacts in this sample, unlike nearby Piece 5 (see Fig. F8, p. 17). Width of view = 1.4 mm; ordinary light.

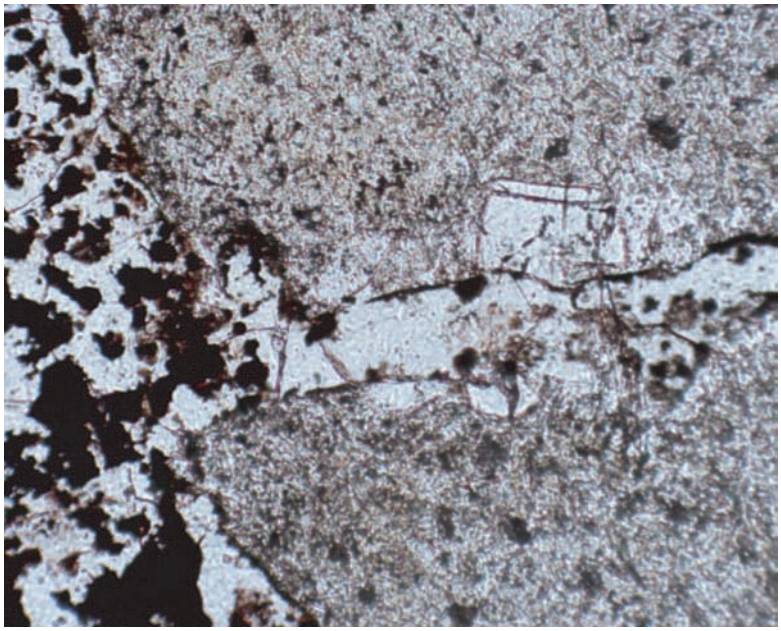

Figure F11. Contact of a jasperoid vein (lower right) cutting altered perlite wallrock fragment (with plagioclase phenocrysts and disseminated pyrite) in Sample 193-1189B-6R-1 (Piece 2, 13–15 cm). Hematite inclusions are exceptionally abundant in this vein and adjacent jasperoid matrix. Width of view = 2.8 mm; ordinary light.

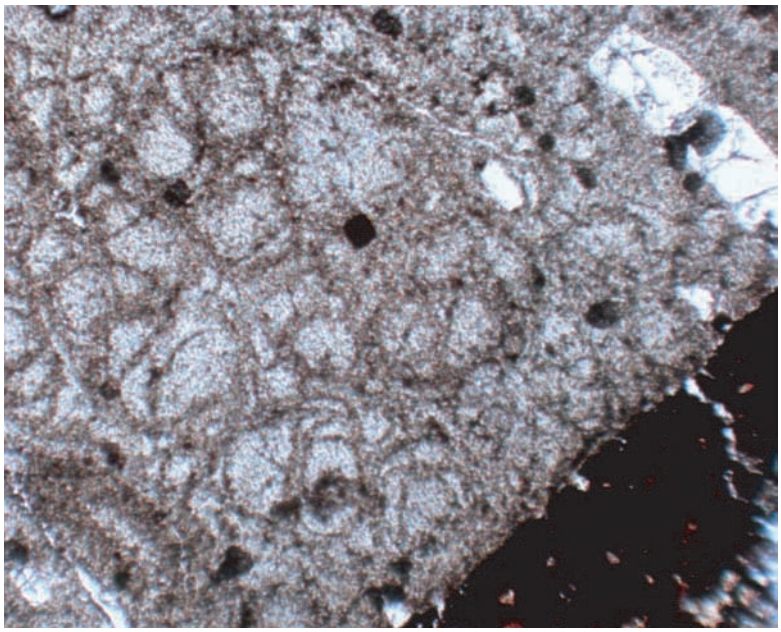

Figure F12. Frondlike growths of hematite included within coarse-grained quartz (with trails of fluid inclusions) in jasperoid Sample 193-1189B-11R-1 (Piece 3, 14–16 cm; CSIRO 142714). The frond structure extends across quartz crystals and apparently predates growth of the latter. Width of view = 1.3 mm. **A.** Ordinary light. **B.** Crossed polarizers.

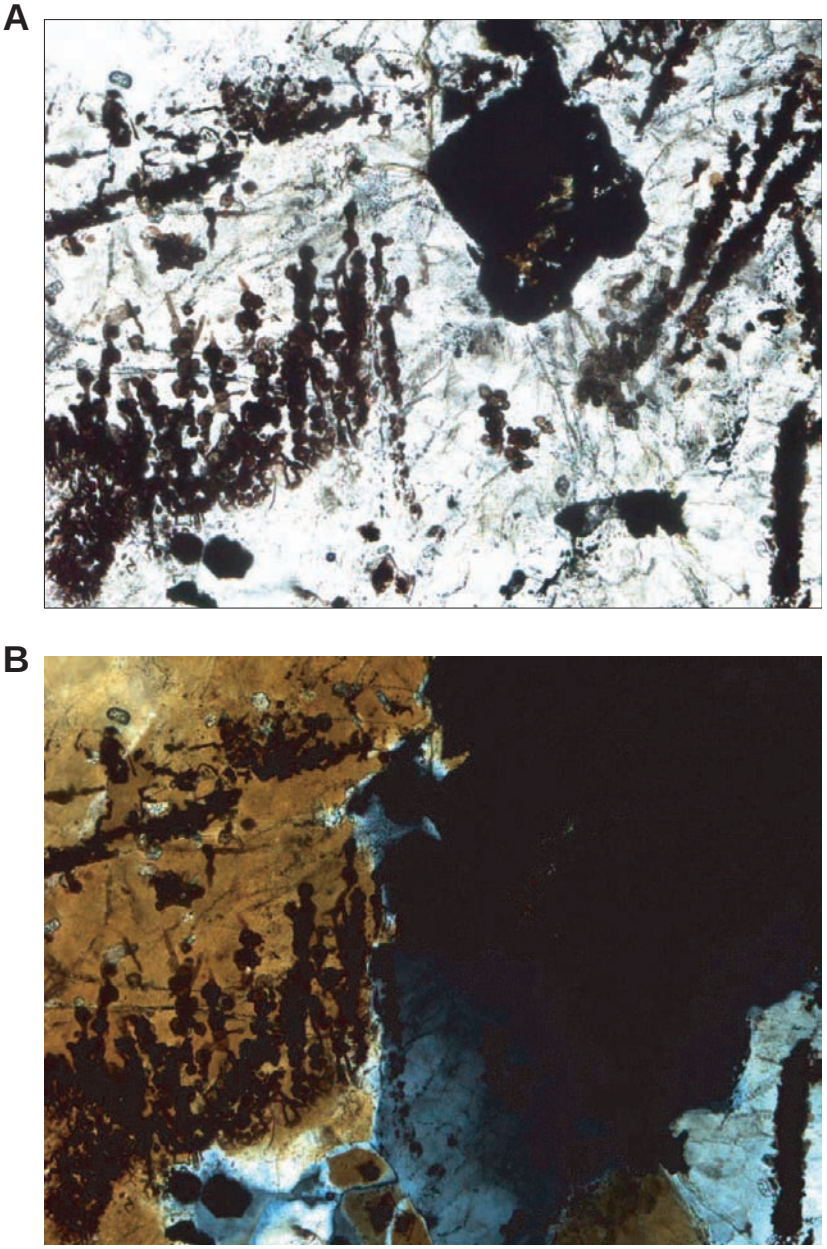

Figure F13. Enlarged view of hematite fronds in jasperoid Sample 193-1189B-11R-1 (Piece 3, 14–16 cm; CSIRO 142714; see Fig. F12, p. 21). The dark fronds are planar and dip steeply into the section. They are aggregates of very thin hematite flakes with subround outlines as seen on the right. Some transparent flakes are orange colored and possibly goethite, but the bright red reflectivity of the sample indicates presence of much hematite. Two tiny apatite prisms are included in quartz at the upper left. Width of view = 0.25 mm; ordinary light.

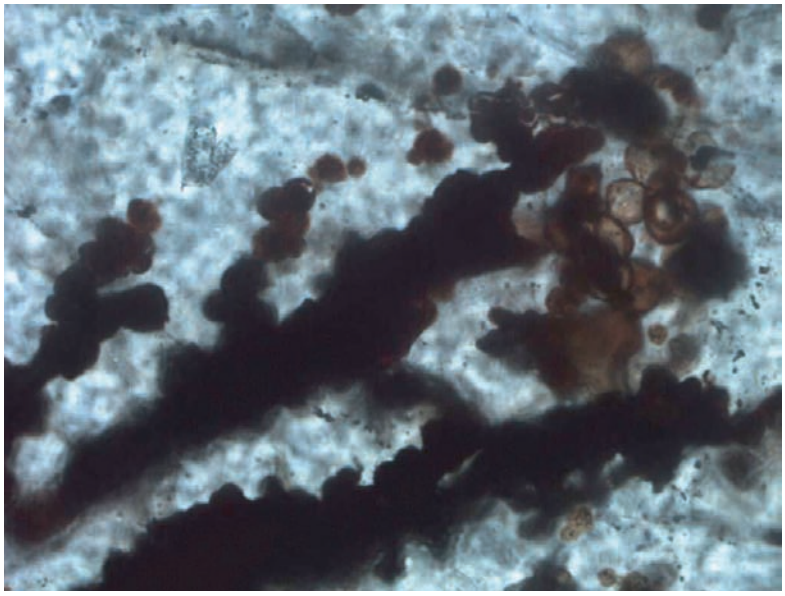

Figure F14. Hematite fronds and an oval growth suggestive of a former botryoidal cavity lining, apparently overgrown by polycrystalline quartz in jasperoid Sample 193-1189B-11R-1 (Piece 3, 14–16 cm; CSIRO 142714). An anhedral pyrite grain at the left has grown across the contact of a wallrock fragment (lower left). Width of view = 1.3 mm. **A.** Ordinary light. **B.** Crossed polarizers.

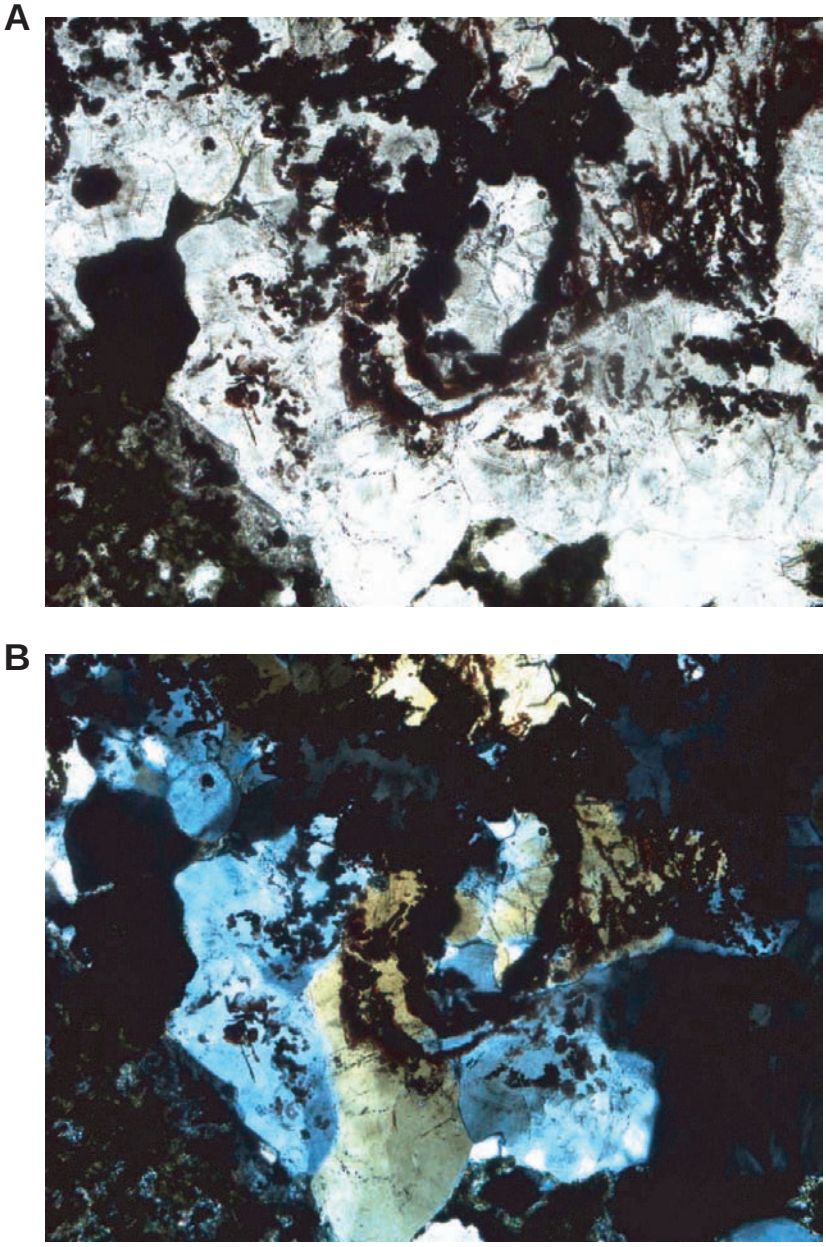

Figure F15. Euhedral growth structure defined by slight variations in refractive index and in places by minute fluid inclusions, in quartz grains within jasperoid Sample 193-1189B-11R-1 (Piece 3, 14–16 cm; CSIRO 142714). The two central quartz grains have distinct cores with abundant inclusions of tiny hematite flakes. Pyrite interstitial to quartz at the lower center possibly fills a former drusy cavity. Elsewhere in the sample, similar quartz grains project into open cavities. The spotty effect arises from the underlying ground surface, caused by use of a narrow aperture for the photograph. Width of view = 0.25 mm; ordinary light.

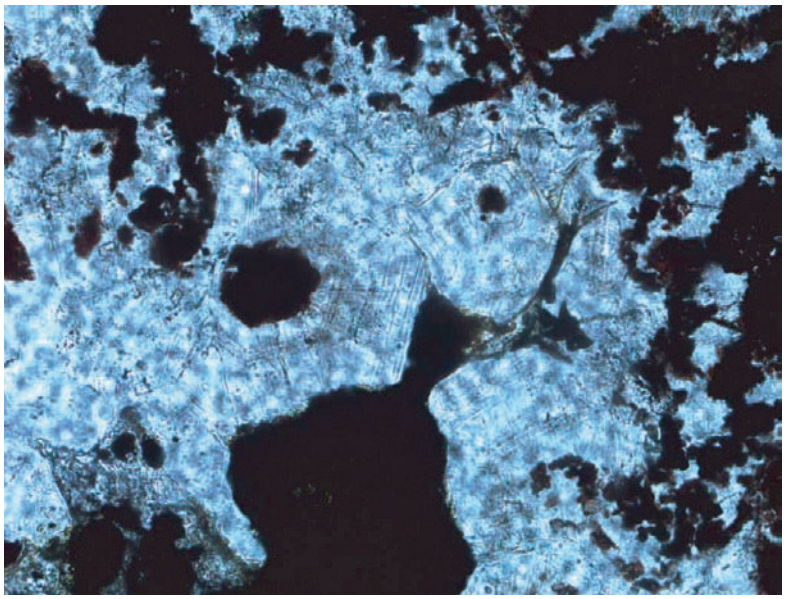

Figure F16. Altered dacite wallrock fragment (top) containing abundant pyrite, with a thin quartz filled fracture extending from the jasperoid host in Sample 193-1189B-11R-1 (Piece 3, 14–16 cm; CSIRO 142714). Pyrite is also common in quartz to the left of the fragment. Birefringent anhydrite fills a former drusy cavity. This sample does not contain selvages of inclusion-free quartz at the margins of wallrock fragments. Width of view = 1.3 mm. **A.** Ordinary light. **B.** Crossed polarizers.

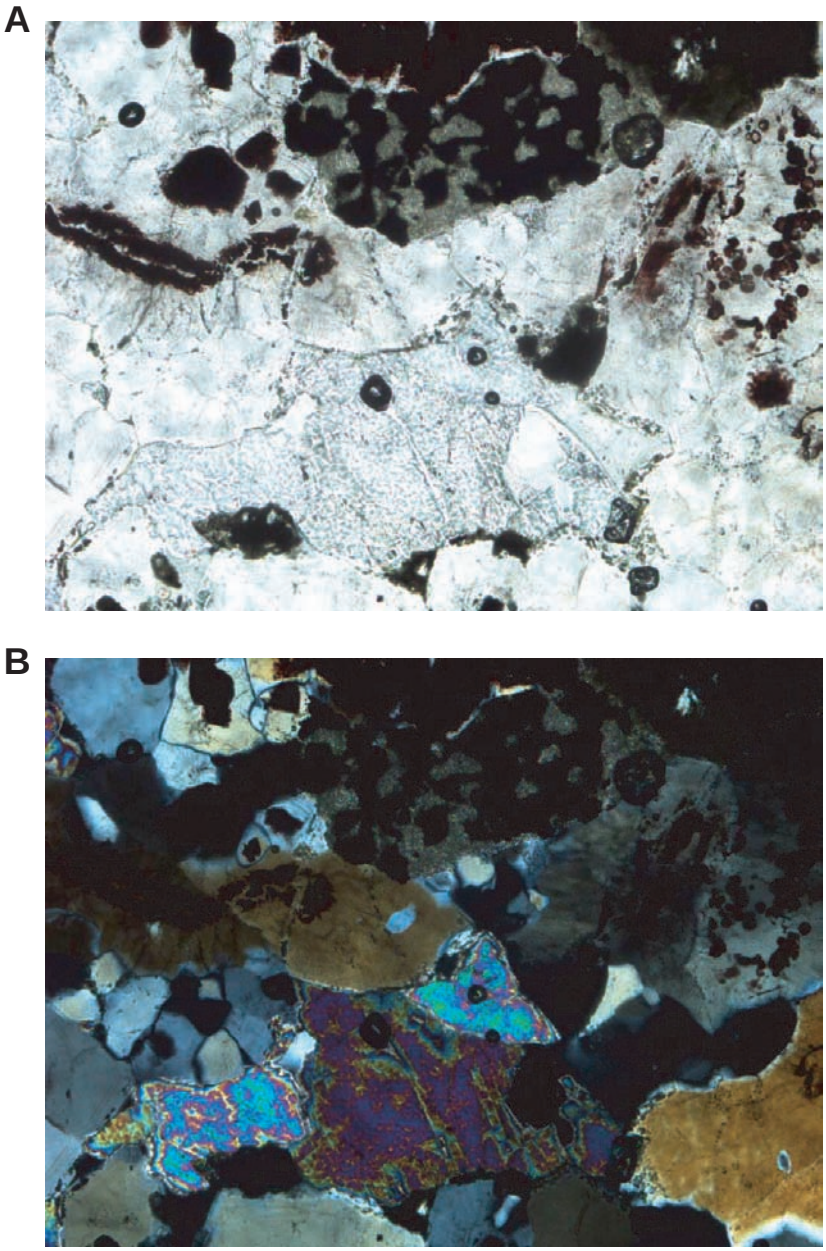

Figure F17. Chondrite-normalized REE patterns. **A**. Jasperoids from Site 1189. **B.** Altered dacite wallrock fragments in breccias close to the Leg 193 jasperoid intersections. **C.** Seabed Fe-Mn-Si deposits at Roman Ruins (from Binns et al., 2002, plus additional data).

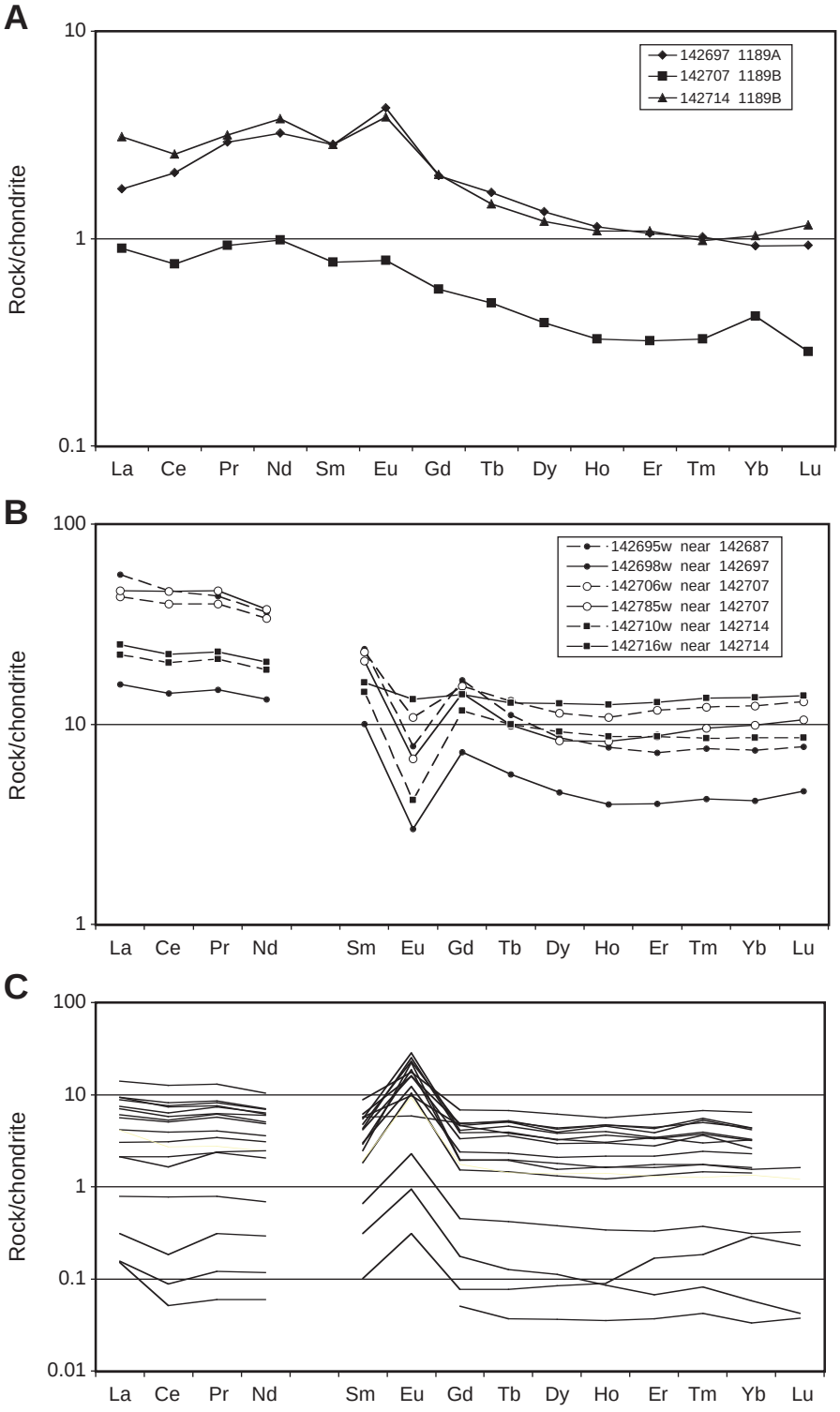

Figure F18. Composition (atom % Si-Fe-Mn) of jasperoid veins from Site 1189 (solid squares), compared to seabed deposits of Fe oxyhydroxide/nontronite/opal (open triangles), Mn oxide (solid circles), and mixed Fe-Mn oxides (open squares) at PACMANUS (from Binns et al., 2002, plus additional data).

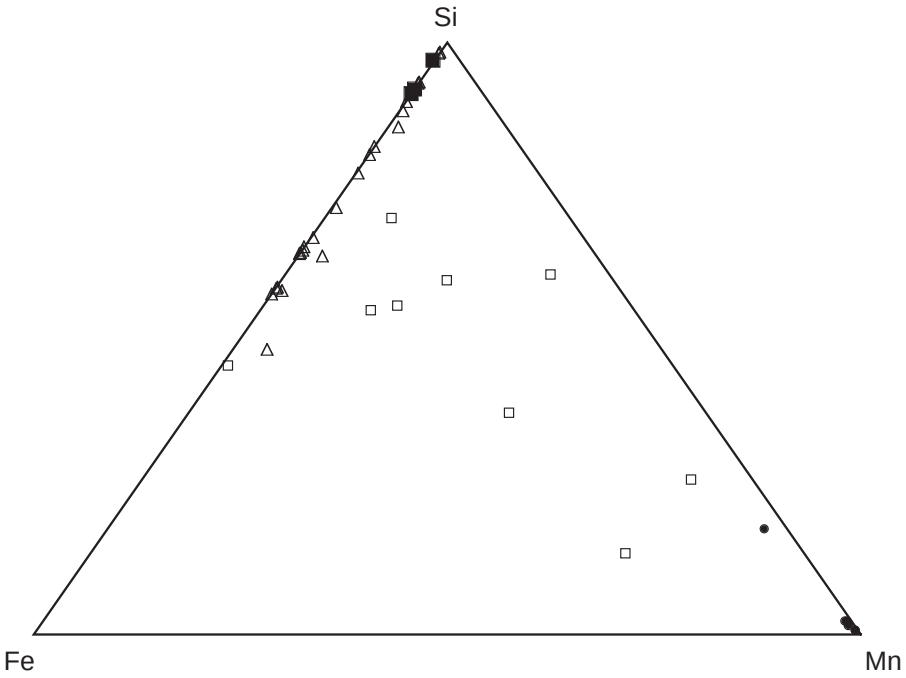

Table T1. Jasperoid sample details.

CSIRO Number	Core, section, piece, interval	Curated depth (mbsf)	Description
142697	193-1189A-7R-1 (Piece 17, 99–102 cm)	59.14	Jasperoid matrix of a breccia with ragged fragments to 1 cm across of soft greenish white altered volcanic rock (Fig. **F2,** p. 11). Jasperoid consists mainly of closely packed, relatively fine grained quartz (~40? m) with distinct cores clouded by minute hematite flakes (diameter < 2? m) and outgrowth margins relatively free of inclusions (Figs. **F3,** p. 12; **F4,** p. 13). Contains numerous tiny and some larger irregular cavities (Figs. **F2,** p. 11; **F3,** p. 12; **F4,** p. 13) and a prominent fracture (Fig. **F5,** p. 14) lined mostly by terminated quartz crystals with fewer or no central inclusions, locally by subhedral to euhedral pyrites, and rarely by late-stage euhedral anhydrite blades. Relatively common pyrite euhedra and subhedra (0.1–0.2 mm) are also intergrown with quartz in the more compact jasperoid, where they are not so clearly related to drusy structures. Rarer ragged patches of chalcopyrite occur in similar positions. Narrow selvages (100–200? m) of clear quartz surrounding wallrock fragments (Figs. **F6,** p. 15; **F7,** p. 16) appear contemporary with quartz in the smaller druses and also with thin quartz veinlets cutting some fragments (Fig. **F7,** p. 16). Tiny barite crystals occur in some selvages but are very rare overall (Fig. **F6,** p. 15). At the immediate contact, selvage quartz appears to have replaced the wallrock (Fig. **F7,** p. 16). The wallrock fragment sectioned has phenocrysts and microlites of unaltered plagioclase set in a chlorite-dominated clay matrix.
142707	193-1189B-6R-1 (Piece 5, 45–55 cm)	79.45	Jasperoid matrix of a breccia with numerous cavities and fragments of white, altered wallrock surrounded by 0.5-mm-thick selvages of pale yellow quartz, which also extends as a vein across one fragment (Fig. **F8,** p. 17). Smoky quartz also surrounds some drusy cavities. Pyrite is more scarcely disseminated through the jasperoid, favoring the proximity of wallrock fragments. Nearby Piece 2 (Fig. **F1,** p. 10), used for preparation of shipboard thin section 1189B#116, contains similar jasperoid, but lacks the conspicuous smoky selvages around wallrock fragments. Here the jasperoid consists of mostly close-packed, rather larger quartz grains (~0.5 mm), again with sharply-bounded cores densely clouded with tiny hematite flakes as much as 5 mm in diameter (Fig. **F9,** p. 18). Commonly the cores themselves have the shapes of doubly-terminated prismatic quartz. Jasperoid quartz also forms veins cutting the wallrock fragments, mainly with fewer, but one with more abundant hematite inclusions (Figs. **F10,** p. 19, **F11,** p. 20). Jasperoid quartz also forms veins cutting the wallrock fragments, mainly with fewer, but one with more abundant hematite inclusions (Figs. **F10,** p. 19, **F11,** p. 20). Poikiloblastic quartz with epitaxial orientations to vein quartz locally replaces wallrock adjacent to such veins (Fig. **F10,** p. 19, and also surrounds rare prismatic quartz euhedra (considered replacive rather than phenocrystal) in some wallrock fragments. Rare fresh plagioclase phenocrysts occur in the clay-altered wallrock fragments, some but not all of which display palimpsest perlite structure (Figs. **F10,** p. 19, **F11,** p. 20) or vesicular fabrics.
142714	193-1189B-11R-1 (Piece 3, 14–16 cm)	127.74	Jasperoid fragment with sliver of pale green chloritic and pyrite-rich wallrock on one side, the entire shipboard sample having a more obvious breccia structure with numerous inclusions of clay-altered wallrock showing vague flow banding. Wallrock contacts are irregular. Abundant irregular microdrusy cavities lined by euhedra of quartz, pyrite, and lesser chalcopyrite, some also with anhydrite tablets (more common than in Samples 142697 and 142707) and patches of soft khaki clay. Quartz surrounding these cavities is coarser and relatively clearer than the red quartz forming areas between them, causing a more spotty appearance than in Samples 142607 and 142707. Quartz grain size is highly variable (0.2–1 mm). Larger grains are strained and have seriate outlines; finer grains tend to be euhedral. Strange frondlike planar aggregates of thin hematite flakes (diameter = 15–25?m) occur within larger quartz grains, commonly extending across grain boundaries in a manner suggesting they formed early and became overgrown by the quartz (Figs. **F12,** p. 21; **F13,** p. 22). Oval growths and curved trails of hematite, possibly lining former cavities, also extend across several large quartz grains (Fig. **F14,** p. 23). The smaller quartz euhedra show marked growth zones and tend to have the more typical central cores (also with euhedral habit) clouded by tiny hematite inclusions (Fig. **F15,** p. 24). Tiny barite crystals are rare inclusions in the larger quartz grains (Fig. **F13,** p. 22). The sample lacks the selvages of clear quartz around wallrock fragments seen in Samples 142697 and 142707, but quartz veinlets cut the wallrock inclusion (Fig. **F16,** p. 25).

Note: CSIRO = Commonwealth Scientific and Industrial Research Organization (Australia).

Table T2. Jasperoid compositions and average Fe-Mn-Si deposit at Roman Ruins.

	Major element oxides (wt%)													
	SiO_2	TiO_2	Al_2O_3	FeO(t)	MnO	MgO	CaO	Na_2O	K_2O	P_2O_5	Total S	LOD	LOI	Total
Method:	XRF *ICP-AES*	ICP-AES	XRF *ICP-AES*	XRF *ICP-AES*	XRF *ICP-AES*	XRF *ICP-AES*	XRF *ICP-AES*	XRF *ICP-AES*	XRF *ICP-AES*	XRF *ICP-AES*	ICP-AES	G	G	(majors)
142697	83.57	0.011	0.51	8.49	0.008	0.11	0.27	0.03	0.02	0.166	5.74	0.03	3.83	100.6
142707	*90.62*	0.008	*0.40*	*3.49*	*0.002*	*0.03*	*0.05*	*0.02*	*0.02*	*0.025*	2.69	NA	NA	96.3
142714	82.95	0.003	0.39	9.36	0.013	0.25	0.79	0.02	0.03	0.161	4.28	NA	NA	96.6
Average Roman Ruins	50.7	0.06	1.3	20.0	3.5	0.9*	0.62	2.7*	0.64	0.47	0.22	8.3	9.8	99.1

Table T2 (continued).

	Elements (ppm)														
	Li	Be	Cl	Sc	V	Cr	Co	Ni	Cu	Zn	Ga	Ge	As	Rb	Sr
Method:	ICP-AES	ICP-AES	XRF	ICP-MS	ICP-MS	ICP-MS	ICP-MS	ICP-MS	ICP-AES	ICP-AES	ICP-MS	ICP-MS	ICP-MS	ICP-MS	ICP-AES
142697	11	<2	150	<1	6.9	3.2	24.0	1.2	1620	12	0.6	2.5	3.0	0.28	4
142707	13	<2	NA	<1	3.4	2.2	13.5	2.3	16	24	0.2	1.2	2.5	0.40	2
142714	9	<2	120	<1	14.8	3.1	2.6	1.2	3715	63	0.8	3.1	3.3	0.37	21
Average Roman Ruins	6.4	4.3	3.3%*	1.8	57	5.1	1.5	4.2	312	625	2.9	33	2050	20	134

Table T2 (continued).

	Elements (ppm)													
	Y	Zr	Mo	Cd (ppb)	In (ppb)	Sb	Te (ppb)	Cs (ppb)	Ba	La	Ce	Pr	Nd	Sm
Method:	ICP-MS	ICP-AES	ICP-MS	ICP-MS	ICP-MS	ICP-MS	ICP-MS	ICP-MS	ICP-AES	ICP-MS	ICP-MS	ICP-MS	ICP-MS	ICP-MS
142697	2.6	<2	0.57	31	96	5.1	174	21	21	0.63	1.98	0.40	2.29	0.65
142707	0.74	<2	0.68	76	4	0.7	570	9	22	0.33	0.72	0.13	0.70	0.18
142714	3.4	<2	9.6	208	978	4.1	30	18	70	1.14	2.44	0.43	2.68	0.65
Average Roman Ruins	4.5	8	16†	680†	225	25†	62	3000	1050	1.83	4.09	0.64	2.82	0.79

Table T2 (continued).

	Elements (ppm)													
	Eu	Gd	Tb	Dy	Ho	Er	Tm	Yb	Lu	Tl (ppb)	Pb	Bi (ppb)	Th (ppb)	U (ppb)
Method:	ICP-MS	ICP-MS	ICP-MS	ICP-MS	ICP-MS	ICP-MS	ICP-MS	ICP-MS	ICP-MS	ICP-MS	ICP-MS	ICP-MS	ICP-MS	ICP-MS
142697	0.370	0.62	0.096	0.51	0.097	0.26	0.036	0.23	0.035	44	20.1	309	18	1320
142707	0.068	0.17	0.028	0.15	0.028	0.08	0.012	0.10	0.011	509	5.5	560	19	289
142714	0.335	0.62	0.085	0.46	0.092	0.27	0.035	0.26	0.044	78	11.6	138	10	4504
Average Roman Ruins	1.11	0.85	0.16	0.91	0.21	0.59	0.096	0.59	0.095	3200†	250†	110	150	9250

Notes: XRF = X-ray fluorescence spectrometry, ICP-AES = inductively coupled plasma–atomic emission spectrometry, ICP-MS = inductively coupled plasma–mass spectrometry, G = gravimetric analysis. FeO(t) = total iron as FeO including Fe in hematite, pyrite (of which a minor proportion occurs in wallrock fragments), and scarce wallrock chlorite. S(t) = total sulfur (sulfide + sulfate). LOD = loss on drying at 105°C (samples predried at ~40°C), LOI = loss on ignition at 1050°C. NA = not analyzed. Average Roman Ruins = Fe-Mn-Si deposit (N = 16), from Binns et al. (2002) plus new data. * = most Cl and Na, and about half of Mg from trapped sea salt. † = outliers excluded from the averages (single samples): 9 ppm Cd; 335 ppm Mo; 3.0 wt% Pb (suspected contamination); 685 ppm Sb; 129 ppm Tl.

Table T3. Normative compositions of jasperoids.

CSIRO number	Normative component (wt%)					
	Quartz	Pyrite	Chalcopyrite	Hematite	Anhydrite	Wallrock
142697	81.9	10.8	0.5	3.4	0.7	2.7
142707	91.4	5.3	Trace	1.0	0.1	2.1
142714	81.3	7.2	1.1	6.4	2.0	2.0

Note: CSIRO = Commonwealth Scientific and Industrial Research Organization (Australia).